Mechanical stress compromises multicomponent efflux complexes in bacteria

Lauren A. Genova[a,1], Melanie F. Roberts[b,1], Yu-Chern Wong[b], Christine E. Harper[c], Ace George Santiago[a,2], Bing Fu[a], Abhishek Srivastava[b,3], Won Jung[a], Lucy M. Wang[b,4], Łukasz Krzemiński[a,5], Xianwen Mao[a], Xuanhao Sun[b,6], Chung-Yuen Hui[b], Peng Chen[a,7], and Christopher J. Hernandez[b,c,7]

[a]Department of Chemistry and Chemical Biology, Cornell University, Ithaca, NY 14853; [b]Sibley School of Mechanical and Aerospace Engineering, Cornell University, Ithaca, NY 14853; and [c]Meinig School of Biomedical Engineering, Cornell University, Ithaca, NY 14853

Edited by Steve Granick, Institute for Basic Science, Ulju-gun, Ulsan, South Korea, and approved October 28, 2019 (received for review June 4, 2019)

Physical forces have a profound effect on growth, morphology, locomotion, and survival of organisms. At the level of individual cells, the role of mechanical forces is well recognized in eukaryotic physiology, but much less is known about prokaryotic organisms. Recent findings suggest an effect of physical forces on bacterial shape, cell division, motility, virulence, and biofilm initiation, but it remains unclear how mechanical forces applied to a bacterium are translated at the molecular level. In Gram-negative bacteria, multicomponent protein complexes can form rigid links across the cell envelope and are therefore subject to physical forces experienced by the cell. Here we manipulate tensile and shear mechanical stress in the bacterial cell envelope and use single-molecule tracking to show that octahedral shear (but not hydrostatic) stress within the cell envelope promotes disassembly of the tripartite efflux complex CusCBA, a system used by *Escherichia coli* to resist copper and silver toxicity. By promoting disassembly of this protein complex, mechanical forces within the cell envelope make the bacteria more susceptible to metal toxicity. These findings demonstrate that mechanical forces can inhibit the function of cell envelope protein assemblies in bacteria and suggest the possibility that other multicomponent, transenvelope efflux complexes may be sensitive to mechanical forces including complexes involved in antibiotic resistance, cell division, and translocation of outer membrane components. By modulating the function of proteins within the cell envelope, mechanical stress has the potential to regulate multiple processes required for bacterial survival and growth.

extrusion loading | single-molecule imaging | multicomponent efflux complex | diffusion dynamics | biomechanics

Over 100 y ago the mathematical biologist D'Arcy Thompson in his book *On Growth and Form* argued for the role of physical forces in the development and morphology of organisms using examples including the shapes of wings, bones, shells, and individual cells (1). Physical forces are now recognized as major contributors to embryogenesis (2), tissue healing (3), and the development of disease (4). While the effect of physical forces on cell physiology is well-recognized in eukaryotic systems, physical forces are also believed to be relevant to prokaryotes (5), although much less is known about their role in prokaryotic organisms including bacteria. Bacteria are ubiquitous in the environment and their sensitivity to physical forces has the potential to influence biotechnology, human health, diagnostics, and biofouling.

Bacteria experience a wide range of mechanical stimuli in their environment including changes in osmolarity and hydrostatic pressure, as well as forces associated with adhesion to surfaces, locomotion, division, turbulent flows, and growth within constrained spaces (6–9). Rapid changes in osmolarity or hydrostatic pressure can influence cell growth and a variety of stretch-activated channels (9), primarily by modulating surface tension in the cell envelope. The mechanical stresses experienced by the bacterial cell envelope during locomotion (10), surface adhesion (8, 11), and cell division (12) are more complicated than those associated with osmolarity and can include combinations of tensile (lengthening), compressive (shortening), and shear (shape-changing) mechanical stresses. How a bacterium responds to these more complicated states of mechanical stress is not well understood.

In eukaryotic systems, the initial transmission of external forces to the cell often occurs through cell surface protein assemblies that cross the cell membrane (13). Bacteria contain many transenvelope protein complexes. In Gram-negative bacteria, transenvelope protein assemblies such as tripartite efflux complexes enable the bacteria to extrude a diverse set of antibiotics and other toxic chemicals, enabling bacterial multidrug resistance (14).

Significance

The field of mechanobiology examines how physical forces modulate cell physiology and has traditionally focused on eukaryotic organisms. Here we show that in bacteria, mechanical stresses can interrupt the structure and function of a molecular assembly used by Gram-negative bacteria to survive and grow in the presence of toxins. This work provides evidence that bacteria, like mammalian cells, can respond to mechanical forces through molecular complexes at the cell surface in ways that are relevant to growth. Our observations further suggest that mechanical forces may be used synergistically with other antimicrobials.

Author contributions: P.C. and C.J.H. designed, conceived, and directed research; L.A.G., M.F.R., Y.C.W., C.E.H., and A.S. performed research; A.G.S., B.F., A.S., W.J., L.M.W., Ł.K., X.M., X.S., and C-Y.H. contributed new reagents or analytic tools; L.A.G., M.F.R., C.E.H., P.C., and C.J.H. analyzed data; L.A.G., M.F.R., P.C., and C.J.H. wrote the paper. L.A.G. prepared cell strains, performed single-molecule imaging, analyzed the mechanical effects on efflux complex assembly, and curated data; M.F.R. fabricated microfluidic devices, performed mechanical manipulation, analyzed cell mechanical stresses, and curated data; Y.-C.W. performed mechanical modeling; L.A.G. and M.F.R. performed cell-growth assays; A.G.S., B.F., W.J., X.M., C.E.H., L.M.W., and Ł.K. contributed to experiments and data analysis; X.S. contributed to microfluidic device design; A.S. contributed to mechanical modeling; C.-Y.H. supervised mechanical modeling; and L.A.G., M.F.R., Y.-C.W., C.E.H., P.C., and C.J.H. analyzed and discussed results and wrote the paper.

The authors declare no competing interest.

This article is a PNAS Direct Submission.

[1]L.A.G. and M.F.R. contributed equally to this work.

[2]Present address: Department of Microbiology and Immunobiology, Harvard Medical School, Boston, MA 02115.

[3]Present address: Corporate Research Laboratory, Advanced Modeling and Simulation Group, 3M Company, St. Paul, MN 55107.

[4]Present address: Department of Mechanical Engineering, Stanford University, Stanford, CA 94305.

[5]Present address: Department of Biology, OncoArendi Therapeutics SA, 02-089 Warsaw, Poland.

[6]Present address: Department of Physiology and Neurobiology, University of Connecticut, Storrs, CT 06269.

[7]To whom correspondence may be addressed. Email: pc252@cornell.edu or cjh275@cornell.edu.

This article contains supporting information online at https://www.pnas.org/lookup/suppl/doi:10.1073/pnas.1909562116/-/DCSupplemental.

First published November 26, 2019.

CusCBA is a tripartite Cu^+ and Ag^+ efflux complex in *Escherichia coli* and belongs to the resistance–nodulation–division family complexes that provide clinically relevant multidrug resistance to Gram-negative bacteria (14). CusA is a trimeric proton-motive-force–driven pump located in the inner membrane; CusB is a periplasmic adaptor protein; CusC is a trimeric outer-membrane pore protein. These three proteins assemble into the complete $CusC_3B_6A_3$ complex to enable efflux of Cu^+/Ag^+ from the cell (15–17). By tagging CusA with a photoconvertible fluorescent protein and using single-molecule tracking measurements, we previously found that inside cells, CusCBA exists in a dynamic equilibrium between an assembled and disassembled state, and this equilibrium is responsive to environmental increase of copper concentration and shifts toward the assembled state for effective efflux in defending against metal (e.g., copper) stress (18).

Here we use a microfluidic system to generate combinations of tension, compression, and shear within the bacterial cell envelope to study the effects of mechanical stress on the function of protein complexes that span the envelope of Gram-negative cells. We demonstrate that cell envelope mechanical stress promotes disassembly of the CusCBA complex in *E. coli* cells and thereby enhances copper-induced reductions in cell reproduction and growth. We further show that the reduced assembly of CusCBA is not associated with tensile/compressive stresses (the primary form of stress generated by osmolarity and hydrostatic pressure) but is correlated with octahedral shear stresses within the cell envelope.

Results and Analysis

Extrusion Loading Provides Controlled Mechanical Stress on Individual Bacteria. To query the contributions of mechanical stress to bacterial physiology, we used a microfluidic device with submicrometer features to apply mechanical loads to individual bacteria. The device is analogous to micropipette aspiration commonly used to study mammalian cell biomechanics (19, 20) but instead of pulling the cell into a tapered channel, the device forces cells into tapered channels using fluid pressure (21). Each device contains sets of tapered channels to apply 12 distinct magnitudes of pressure difference (ΔP) across the trapped bacteria within a single experiment (Fig. 1 *A* and *B* and *SI Appendix*, Fig. S1). The pressure difference is controlled by modifying fluid pressure at the inlet (also affecting the average pressure, P_{ave}, which is indicative of hydrostatic pressure experienced by the cell) and determined locally with hydraulic circuit models (*SI Appendix*, section 1.2). We refer to this loading modality as "extrusion loading." Bacteria submitted to stepwise increases in ΔP exhibited increases in cell length and decreases in cell width, resulting in a net reduction in cell volume (Fig. 1*C* and *SI Appendix*, Fig. S4). Analytical and finite-element models indicate that extrusion loading causes increases in axial tensile stress and reductions in hoop (transverse) tensile stress, related to the magnitude of ΔP (Fig. 1*D* and *SI Appendix*, Figs. S5 and S6). Furthermore, analytical examination shows that reductions in cell volume during extrusion loading result in an increase in cell internal pressure, which we attribute to increases in osmolarity associated with loss of water from the cytoplasm when cell volume declines.

Mechanical Stress from Pressure Differentials Disrupts the Assembly of CusCBA in the Cell. To understand the effects of mechanical stress on a transenvelope complex, we examined the assembly of CusCBA in *E. coli* cells under extrusion loading (Fig. 1*B*). When assembled, CusCBA forms a rigid link across the cell envelope and is therefore subject to mechanical stress and strain experienced by the cell envelope. To probe the assembly of CusCBA,

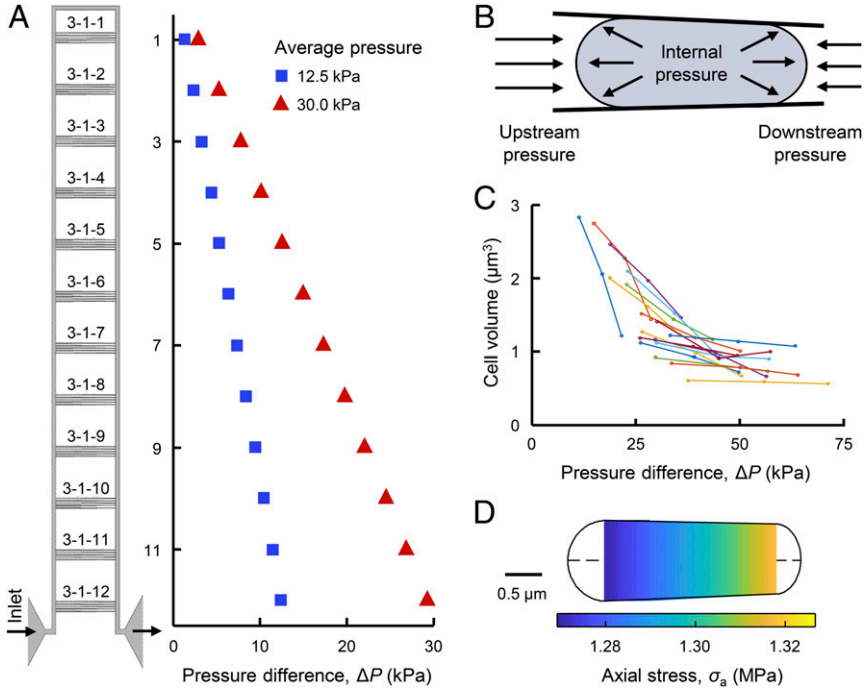

Fig. 1. Mechanical loading of bacteria via a microfluidic device. (*A*) A functional unit of the microfluidic device has 12 sets of 5 tapered channels. Fluid flow enters the functional unit at the bottom left, travels around the bypass channel, and exits out the bottom right. The difference between upstream and downstream pressure is larger for tapered channels closer to the inlet and outlet. Increasing the applied pressure increases the pressure difference ΔP at each set of tapered channels (and also increases the average pressure, P_{ave}). (*B*) Trapped bacteria experience greater upstream pressure than downstream pressure. The pressure difference ΔP is defined as the difference between the upstream and downstream pressures. Internal pressure due to turgor is also present. (*C*) Increases in ΔP via stepwise increases of externally applied pressure results in reduced cell volume of trapped cells. Lines connect measurements of same cells. (*D*) Analytical modeling of a trapped cell indicates a linear increase in axial tensile stress along the length of the cell.

we tagged the C terminus of the inner-membrane protein CusA by a photoconvertible fluorescent protein mEos3.2 (i.e., CusA^{mE}) at its chromosomal locus (*SI Appendix*, section 1.7); this tagging ensures physiological expression of CusA^{mE} in the cell. This fluorescent protein tag also enables the use of sparse photoconversion and subsequent time-lapse stroboscopic fluorescence imaging to track the motions of individual photoconverted CusA^{mE} proteins at 10s of nanometer precision and 60-ms time resolution (Fig. 2 *B*, *Inset*) and quantify CusA^{mE} copy number in each cell (18).

We examined hundreds of cells submitted to extrusion loading containing, in total, thousands of CusA^{mE} proteins. These cells were in different tapered channels and sampled a large range of ΔP (Fig. 2*A*), allowing us to sort the cells into groups of similar ΔP and determine the relationship between the magnitude of extrusion loading and diffusive behaviors of tracked CusA^{mE} proteins. Within assembled CusCBA complexes, the motion of CusA^{mE} is severely restricted to be almost stationary, but CusA^{mE} that is disassembled from the complex is highly mobile. These 2 diffusive states of CusA^{mE} can be differentiated by analyzing the distribution of CusA^{mE}'s single-molecule displacement lengths between adjacent image frames (Fig. 2*B* and *SI Appendix*, section 1.12) (18). After using an inverse transformation approach to deconvolute the effects of cell confinement and 2D projection of 3D motions (18, 22, 23), we could resolve the displacement length distribution into the two diffusive states across all applied pressure conditions: the stationary assembled state and the mobile

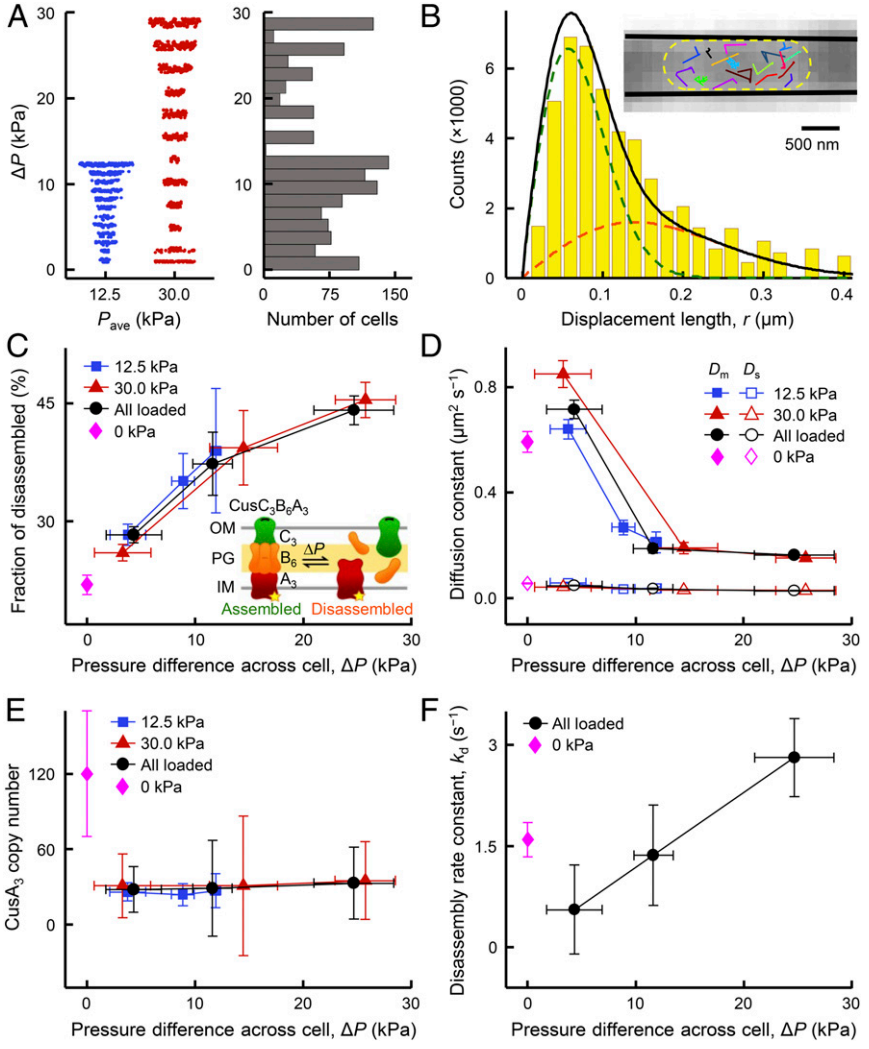

Fig. 2. Single-molecule tracking uncovers mechanical-stress-induced CusCBA disassembly. (*A*) Cells were examined at 2 applied external loading conditions resulting in average pressure values of 12.5 kPa ($n = 592$ cells; blue points) and 30.0 kPa ($n = 732$ cells; red points), giving a range of ΔP across individual cells. (*B*) Distribution of displacement length r per time lapse for single CusA^{mE} proteins at $P_{ave} = 30.0$ kPa and $\Delta P = 24.7 \pm 3.7$ kPa, in which the cell confinement effect is deconvoluted (*SI Appendix*, section 1.12). The distribution here resolves minimally 2 Brownian diffusion states (*SI Appendix*, Eq. **S23**): a mobile disassembled state (orange dashed line) and an almost stationary-assembled state (green dashed line), with diffusion constants of $D_m = 0.16 \pm 0.01$ μm^2 s^{-1} and $D_s = 0.027 \pm 0.001$ μm^2 s^{-1} and fractional populations of $A_m = 44 \pm 2\%$ and $A_s = 56 \pm 2\%$, respectively. Solid black line: overall fit. (*Inset*) Overlay of many position trajectories of single CusA^{mE} proteins in a living *E. coli* cell trapped in a tapered channel. Each colored line is from 1 CusA^{mE}. Yellow dashed line: cell boundary; solid black lines: inner walls of the tapered channel. (*C*) Fractional populations of the mobile disassembled state of CusA^{mE} increases with increasing ΔP at $P_{ave} = 30.0$ kPa (red) or 12.5 kPa (blue). Black: results combining $P_{ave} = 30.0$- and 12.5-kPa conditions. Magenta: results where $P_{ave} = 0$ and $\Delta P = 0$. Color coding of points applies to *D*–*F* as well. (*Inset*) CusCBA can dynamically shift between 2 forms: assembled (stationary, left) and disassembled (mobile, right). OM, outer membrane; PG, peptidoglycan; IM, inner membrane. Yellow star: mEos3.2-tag on CusA. (*D*) The diffusion constants of the mobile disassembled state (D_m) and the stationary-assembled state (D_s) vs. ΔP at different pressure conditions. (*E*) Copy number of CusA trimers ($CusA_3$) vs. ΔP at different pressure conditions. (*F*) Effective disassembly rate constant k_d vs. ΔP at different pressure conditions. Error bars are SD, and lines connecting the points are eye guides in *C*–*F*. Numerical values reported here are in mean ± SD.

disassembled state, along with diffusion constants and fractional populations (Fig. 2*B* and *SI Appendix*, Fig. S11*C*). The resolution and assignment of these two diffusion states were validated previously by control measurements on the free mEos3.2 tag, single-deletion strains missing CusC or CusB, and diffusion simulations (18).

Strikingly, the fractional population of the mobile disassembled state of $CusA^{mE}$ in the cell increases by a factor of ∼2 when ΔP increases from ∼4 to ∼25 kPa (Fig. 2*C*), indicating a direct association between the magnitude of extrusion loading and the disruption of CusCBA assembly in the cell. Concurrently, the effective diffusion constant of the mobile disassembled $CusA^{mE}$ decreases by a factor of ∼4 across this range of ΔP, while that of the stationary assembled CusCBA complex, which traverses the cell envelope, remains the same, as expected for stationary objects (Fig. 2*D*). We further conducted experiments where the applied pressure is zero and ΔP is thus also zero on the trapped cells. The determined fractional population and diffusion constant of the mobile disassembled $CusA^{mE}$ remain on the same trends vs. ΔP (Fig. 2 *C* and *D*). These trends show that external mechanical stress can influence the assembly of the CusCBA complex as well as the diffusivity of mobile unassembled inner-membrane proteins, the latter of which could have contributions from membrane fluidity changes from mechanical stress (24).

Bacteria submitted to extrusion loading experience a pressure difference across the tapered channels (ΔP), as well as a hydrostatic pressure (P_{ave}, the average between upstream and downstream pressures on a cell), both related to the fluid pressure applied at the device inlet. While the behaviors of $CusA^{mE}$ in response to ΔP were substantial, the behaviors of $CusA^{mE}$ showed no significant differences when P_{ave} changed by a factor of 2 (Fig. 2 *C* and *D*, blue vs. red points); combining results from the two P_{ave} conditions gave the same behaviors (Fig. 2 *C* and *D*, black points). Therefore, hydrostatic pressure, at least within our experimental regime, does not play significant roles in membrane protein assembly and diffusivity, suggesting that mechanically induced disassembly of CusCBA would not be observed using osmotic shock or hydrostatic pressure, two commonly used mechanical stimuli that primarily modify surface tension (25).

We further examined the copy number and spatial distribution of $CusA^{mE}$ in all cells across the different pressure conditions. Neither of these two properties show noticeable changes with varying ΔP or P_{ave} under applied pressure conditions (Fig. 2*E* and *SI Appendix*, Fig. S14), supporting the idea that modifications in CusCBA assembly induced by extrusion loading are likely not due to cell physiological changes such as CusA protein expression or intracellular localization.

We further analyzed the single-molecule displacement vs. time trajectories of $CusA^{mE}$ to estimate the underlying kinetics of $CusA^{mE}$ disassembly from the CusCBA complex. In these trajectories, transitions from small displacements to large ones predominantly reflect disassembly events (*SI Appendix*, Fig. S12 and section 1.13). The extracted effective disassembly rate constant increases from ∼0.5 to ∼2.8 s^{-1} with increasing ΔP (Fig. 2*F*), supporting the idea that mechanical stress compromises the stability of the assembled CusCBA complex in part by enhancing the disassembly rate. In the absence of applied pressure where ΔP is also zero for all cells in the tapered channels, the effective disassembly rate constant as well as the copy number of $CusA^{mE}$ are slightly higher than those under applied pressures, but the differences are within or close to experimental errors (Fig. 2 *E* and *F*).

Mechanical Stress Enhances Cell Sensitivity to Copper Stress. Copper and silver are toxic to *E. coli*, impeding cell growth at low to moderate concentrations and causing cell death at high concentrations. CusCBA plays a crucial role in *E. coli*'s ability to resist the presence of copper (and silver) ions in the environment (17). The mechanical-stress-induced disassembly of CusCBA in the cell should therefore lead to a further reduction in cell growth under copper stress conditions. To confirm such functional effects, we examined how mechanical stress in extrusion loading affected elongation and reproduction of hundreds of individual *E. coli* cells by tracking cell length and time to division under copper stress. Rate of elongation and time to division were both examined in media with 0 or 2.5 mM $CuSO_4$ (*SI Appendix*, Figs. S16 and S17). The maximum rate of elongation decreased with larger magnitudes of extrusion loading (greater ΔP, Fig. 3*A*) and followed an exponential decay, consistent with known adverse effect of mechanical stress on bacterial growth (26–28). In the presence of copper stress, the exponential decay rate (0.38 ± 0.14 kPa^{-1}, value ± SE) was substantially greater than that without copper stress (0.08 ± 0.04 kPa^{-1}, $P = 0.048$), indicating synergy between mechanical and copper stress in suppressing cell elongation (or division) (Fig. 3*A*). It is worth noting that the indiscernible difference with or without copper at ΔP greater than ∼20 kPa is due to a saturation effect—the growth has slowed by mechanical stress to an extent that additional copper stress would make little difference.

To confirm that the effects of mechanical stress on the function of CusCBA were not limited to extrusion loading in microfluidic chambers, we also assessed the effects of copper stress using an alternative mechanical loading approach: the growth of cells encapsulated in agarose gel with increasing stiffness (28, 29). We used 3 different concentrations of agarose (0, 0.25, and 0.5 wt/vol %), corresponding to 3 different levels of gel stiffness (*SI Appendix*, Fig. S13 and section 1.14) (it is worth noting that at agarose concentrations smaller than 0.25%, the solution does not form gels). The maximum growth rate of the *E. coli* population decreased in higher agarose concentration gels, consistent with a previous report (29) (Fig. 3*B*, black points). Expectedly, the presence of copper also decreases the cell-growth rate (e.g., pink vs. black points in Fig. 3*B*). More important, in gels that impose mechanical resistance on cell growth, the copper-induced decrease in growth rate is greater in magnitude than that in the absence of gels (e.g., pink and black points at 0.25% vs. at 0.0% agarose in Fig. 3*B*), indicating that mechanical stress enhances the toxic effects of copper ions on growth. It is worth noting that such agarose gel encapsulation does not restrict nutrient access to the cells (28, 29). Taken together, the results from extrusion loading and agarose gel embedding support the idea that mechanical-stress-induced disassembly of CusCBA enhances the toxic effects of copper stress on bacterial physiology.

Role of Shear Stress within the Cell Envelope. Extrusion loading and gel encapsulation techniques generate substantially different combinations of tensile, compressive, and shear stresses in the bacterial cell envelope (*SI Appendix*, section 1.6). To better understand the components of cell envelope stress associated with mechanically enhanced disassembly of CusCBA and resulting enhancement of copper sensitivity, we generated analytical and finite-element models of the 2 mechanical loading modalities (*SI Appendix*, sections 1.5 and 1.6). Extrusion loading increases axial tension and reduces tensile hoop stresses while gel encapsulation reduces axial tension in the cell envelope with little effect on hoop stresses (*SI Appendix*, Fig. S6*C*).

To identify the forms of mechanical stress that promote disassembly of CusCBA, we decomposed the 3D stress state within the cell envelope into a hydrostatic (volume-changing) component and an octahedral shear (shape-changing) component (Fig. 3 *C*, *Inset*). Hydrostatic stress in the cell envelope is known to affect molecular processes like stretch-activated channels, however, in extrusion loading, hydrostatic stresses in the cell envelope showed only a small increasing trend with increasing ΔP, whereas in gel encapsulation an opposite trend was observed (*SI Appendix*, Fig. S7). The lack of concurrence between the two loading modalities suggests that hydrostatic stress is not likely the

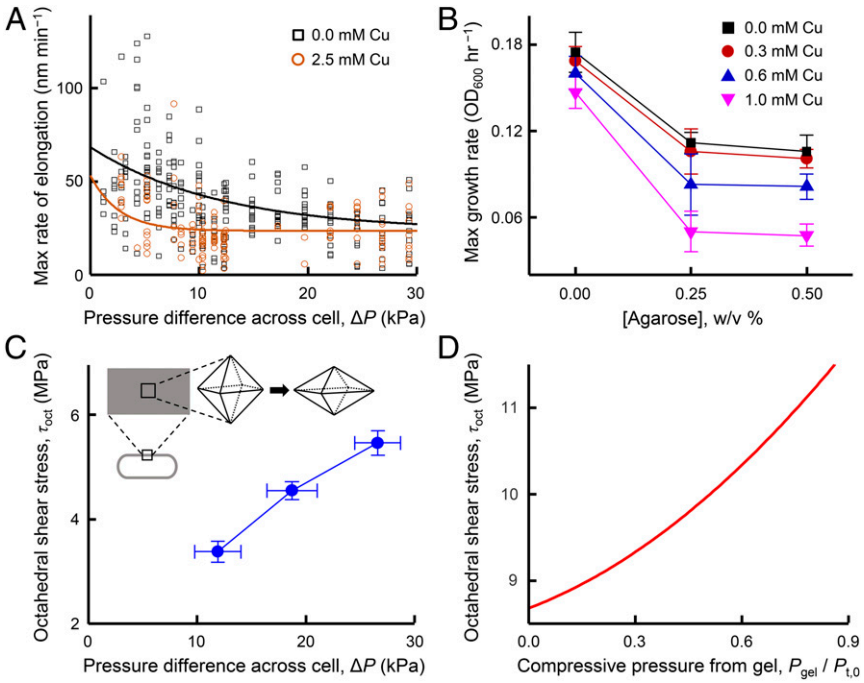

Fig. 3. Mechanical loading enhances the toxic effects of copper stress on elongation and growth of *E. coli*. (*A*) Maximum growth rate (elongation) of individual cells under extrusion loading without copper stress ($n = 253$ cells) and with copper stress ($n = 134$ cells). Solid lines display exponential decay fits that differ between groups ($P = 0.048$). (*B*) Maximum growth rate of cells encapsulated in agarose gel without and with increasing copper stress. Maximum growth rate is influenced by copper concentration, agarose stiffness (concentration), and copper*agarose ($P = 0.046$ for all copper concentrations at 0% and 0.25% agarose conditions), indicating synergy between copper concentration and agarose stiffness (*SI Appendix*, section 1.14). Error bars are SD. (*C*) Finite-element analysis demonstrates that octahedral shear stress in the cell envelope of bacteria under extrusion loading increased with increasing ΔP. Material properties used in the analysis are in *SI Appendix*, Table S3. Error bars are SD. (*Inset*) Three-dimensional depictions of the effects of octahedral shear stress on an infinitesimal element located in the cell envelope. The volume does not change but the shape is distorted (compared with hydrostatic stresses, *SI Appendix*, Fig. S7 *A*, *Inset*). (*D*) Octahedral shear stress in the cell envelope of bacteria encapsulated in gel (growth confinement loading) increased with increasing compressive pressure from the gel (P_{gel}). The compressive pressure was normalized to the assumed turgor pressure ($P_{t,0}$), where a value of $P_{gel}/P_{t,0}$ greater than 1.0 would result in buckling or collapse of the cell.

main cause of the mechanically induced disassembly of CusCBA; this assertion is supported by the fact that CusCBA disassembly during extrusion loading was insensitive to variation in hydrostatic pressure (P_{ave}, which primarily regulates cell envelope hydrostatic stress). In contrast, mechanical loading through both extrusion loading and gel encapsulation lead to large increases in cell envelope octahedral shear stress (Fig. 3 *C* and *D*), suggesting that octahedral shear stress is a likely contributor to disassembly of CusCBA. In materials science, octahedral shear stress is often a useful predictor of material failure. We postulate that octahedral stress within the cell envelope, by promoting distortion of the cell envelope, can facilitate separation of the components of CusCBA and/or modulate the assembly–disassembly kinetics. Moreover, the total strain energy imposed on the entire cell envelope during extrusion loading or in gel encapsulation was on the order of 10^{-18} to 10^{-13} kcal, more than sufficient to overcome the energy needed to disrupt all CusCBA complexes in a cell (about 10^{-24} to 10^{-23} kcal; *SI Appendix*, section 3).

Discussion

Using extrusion loading and single-molecule imaging of individual *E. coli* cells, we have discovered that mechanical stress on the cell disrupts the assembly of CusCBA, a tripartite metal efflux pump that is crucial for resistance to toxic metals, thereby enhancing the effects of copper stress on cell growth. Our finding that octahedral shear stresses (but not hydrostatic stresses) within the cell envelope influence molecular mechanisms further suggests that mechanical loading modalities that primarily generate hydrostatic stress in the cell envelope (e.g., osmotic shock and other variations in turgor pressure; *SI Appendix*, Fig. S8) may stimulate only a subset of mechanosensitive mechanisms in bacteria (30). Octahedral shear stresses can develop in the cell envelope following a number of common mechanical events experienced by bacteria in the environment including adhesion to surfaces, overgrowth within crowded cavities, and locomotion. Furthermore, octahedral shear stresses have long been recognized as having distinct effects on physiology; in mammalian systems, octahedral shear stresses have been recognized as having effects on cell, tissue, and organ physiology that are distinct from hydrostatic stresses (13, 31). Our findings suggest a broader role for cell envelope stresses in bacteria. Lastly, our findings demonstrate that mechanical stress in the cell envelope can influence transenvelope protein complexes resulting in physiological changes in bacteria. Transenvelope protein complexes are ubiquitous in Gram-negative bacteria and their functions include regulating antibiotic resistance (14, 32, 33), cell division (34), and the translocation of outer-membrane components (35). Similar effects of mechanical stresses on these other classes of transenvelope complexes would suggest that many more physiological mechanisms in bacteria can be sensitive to mechanical forces.

Materials and Methods

Materials and methods are described in *SI Appendix*, section 1. These include fabrication and characterization of the microfluidic device, device loading, strain construction (36, 37), imaging sample preparation, procedures of single-molecule imaging/tracking (38–44) and single-cell protein

quantification (18, 45), image and data analysis, and agarose embedding assay of cell growth.

Statistical Information. Differences among groups were identified using two-tailed ANOVA. Differences between trends were determined using analysis of covariance (ANCOVA) to account for the effects of covariates. Where appropriate, data were submitted to logarithmic transformation to achieve normal distributions. Least-squares regression models were generated to describe trends. Exponential decay rates are determined from nonlinear regression fits to $y = a_0 + a_1 e^{-x\tau}$, where τ is the decay rate constant (variance noted using SE, e.g., Fig. 3*A*). Unless otherwise stated, statistical tests were performed with $\alpha = 0.05$. For single-molecule imaging results, the data presented included the number of cells measured. SDs are provided in relevant figures and tables for data points and fitted parameters.

Data Availability. The data that support the findings of this study are available from the corresponding authors, P.C. and C.J.H., upon reasonable request.

ACKNOWLEDGMENTS. This study was supported by Army Research Office Grant W911NF-19-1-0121 (P.C. and C.J.H.), NSF Grant CMMI-1463084 (C.J.H.), NIH Grants GM109993 (P.C.), F31AI143208 (L.A.G.), and 5T32GM008500 (L.A.G.). This work was performed in part at the Cornell NanoScale Science and Technology Facility (CNF), a member of the National Nanotechnology Coordinated Infrastructure, which is supported by NSF Grant ECCS-1542081. Imaging on the Andor/Olympus Spinning Disk Confocal at the Biotechnology Resource Center (BRC) was supported by NIH Grant 1S10OD010605. We thank the staff at the CNF and BRC for assistance, F. Yang for helping with imaging experiments, K. Gunsallus for finite-element modeling assistance, and G. Guisado for measurement assistance.

1. D. A. W. Thompson, L. L. Whyte, *On Growth and Form* (The University Press, Cambridge Engineering, 1942).
2. C.-P. Heisenberg, Y. Bellaïche, Forces in tissue morphogenesis and patterning. *Cell* **153**, 948–962 (2013).
3. K. H. Vining, D. J. Mooney, Mechanical forces direct stem cell behaviour in development and regeneration. *Nat. Rev. Mol. Cell Biol.* **18**, 728–742 (2017).
4. T. Panciera, L. Azzolin, M. Cordenonsi, S. Piccolo, Mechanobiology of YAP and TAZ in physiology and disease. *Nat. Rev. Mol. Cell Biol.* **18**, 758–770 (2017).
5. A. W. Orr, B. P. Helmke, B. R. Blackman, M. A. Schwartz, Mechanisms of mechanotransduction. *Dev. Cell* **10**, 11–20 (2006).
6. G. K. Auer, D. B. Weibel, Bacterial cell mechanics. *Biochemistry* **56**, 3710–3724 (2017).
7. J. E. Sanfilippo *et al*., Microfluidic-based transcriptomics reveal force-independent bacterial rheosensing. *Nat. Microbiol.* **4**, 1274–1281 (2019).
8. C. A. Rodesney *et al*., Mechanosensing of shear by *Pseudomonas aeruginosa* leads to increased levels of the cyclic-di-GMP signal initiating biofilm development. *Proc. Natl. Acad. Sci. U.S.A.* **114**, 5906–5911 (2017).
9. E. R. Rojas, K. C. Huang, Regulation of microbial growth by turgor pressure. *Curr. Opin. Microbiol.* **42**, 62–70 (2018).
10. R. Rusconi, J. S. Guasto, R. Stocker, Bacterial transport suppressed by fluid shear. *Nat. Phys.* **10**, 212–217 (2014).
11. A. Siryaporn, S. L. Kuchma, G. A. O'Toole, Z. Gitai, Surface attachment induces Pseudomonas aeruginosa virulence. *Proc. Natl. Acad. Sci. U.S.A.* **111**, 16860–16865 (2014).
12. X. Zhou *et al*., Bacterial division. Mechanical crack propagation drives millisecond daughter cell separation in Staphylococcus aureus. *Science* **348**, 574–578 (2015).
13. D. T. Tambe *et al*., Collective cell guidance by cooperative intercellular forces. *Nat. Mater.* **10**, 469–475 (2011).
14. H. I. Zgurskaya, H. Nikaido, Multidrug resistance mechanisms: Drug efflux across two membranes. *Mol. Microbiol.* **37**, 219–225 (2000).
15. T. D. Mealman, N. J. Blackburn, M. M. McEvoy, Metal export by CusCFBA, the periplasmic Cu(I)/Ag(I) transport system of Escherichia coli. *Curr. Top. Membr.* **69**, 163–196 (2012).
16. C. C. Su *et al*., Crystal structure of the CusBA heavy-metal efflux complex of Escherichia coli. *Nature* **470**, 558–562 (2011).
17. F. W. Outten, D. L. Huffman, J. A. Hale, T. V. O'Halloran, The independent cue and cus systems confer copper tolerance during aerobic and anaerobic growth in Escherichia coli. *J. Biol. Chem.* **276**, 30670–30677 (2001).
18. A. G. Santiago *et al*., Adaptor protein mediates dynamic pump assembly for bacterial metal efflux. *Proc. Natl. Acad. Sci. U.S.A.* **114**, 6694–6699 (2017).
19. R. M. Hochmuth, Micropipette aspiration of living cells. *J. Biomech.* **33**, 15–22 (2000).
20. D. Needham, R. M. Hochmuth, A sensitive measure of surface stress in the resting neutrophil. *Biophys. J.* **61**, 1664–1670 (1992).
21. X. Sun, W. D. Weinlandt, H. Patel, M. Wu, C. J. Hernandez, A microfluidic platform for profiling biomechanical properties of bacteria. *Lab Chip* **14**, 2491–2498 (2014).
22. T. Y. Chen *et al*., Quantifying multistate cytoplasmic molecular diffusion in bacterial cells via inverse transform of confined displacement distribution. *J. Phys. Chem. B* **119**, 14451–14459 (2015).
23. F. Oswald, E. L M Bank, Y. J. Bollen, E. J. Peterman, Imaging and quantification of trans-membrane protein diffusion in living bacteria. *Phys. Chem. Chem. Phys.* **16**, 12625–12634 (2014).
24. N. C. S. Mykytczuk, J. T. Trevors, L. G. Leduc, G. D. Ferroni, Fluorescence polarization in studies of bacterial cytoplasmic membrane fluidity under environmental stress. *Prog. Biophys. Mol. Biol.* **95**, 60–82 (2007).
25. E. R. Rojas *et al*., The outer membrane is an essential load-bearing element in Gram-negative bacteria. *Nature* **559**, 617–621 (2018).
26. R. R. Trivedi *et al*., Mechanical genomic studies reveal the role of D-alanine metabolism in Pseudomonas aeruginosa cell stiffness. *MBio* **9**, e01340–e01318 (2018).
27. F. Wong *et al*., Mechanical strain sensing implicated in cell shape recovery in Escherichia coli. *Nat. Microbiol.* **2**, 17115 (2017).
28. G. K. Auer *et al*., Mechanical genomics identifies diverse modulators of bacterial cell stiffness. *Cell Syst.* **2**, 402–411 (2016).
29. H. H. Tuson *et al*., Measuring the stiffness of bacterial cells from growth rates in hydrogels of tunable elasticity. *Mol. Microbiol.* **84**, 874–891 (2012).
30. C. D. Cox, N. Bavi, B. Martinac, Bacterial mechanosensors. *Annu. Rev. Physiol.* **80**, 71–93 (2018).
31. F. Pauwels, *Biomechanics of the Locomotor Apparatus: Contributions on the Functional Anatomy of the Locomotor Apparatus* (Springer-Verlag, Berlin, 1980).
32. M. D. Routh *et al*., Efflux pumps of the resistance-nodulation-division family: A perspective of their structure, function, and regulation in gram-negative bacteria. *Adv. Enzymol. Relat. Areas Mol. Biol.* **77**, 109–146 (2011).
33. L. J. Piddock, Multidrug-resistance efflux pumps - not just for resistance. *Nat. Rev. Microbiol.* **4**, 629–636 (2006).
34. M. A. Gerding, Y. Ogata, N. D. Pecora, H. Niki, P. A. de Boer, The trans-envelope Tol-Pal complex is part of the cell division machinery and required for proper outer-membrane invagination during cell constriction in E. coli. *Mol. Microbiol.* **63**, 1008–1025 (2007).
35. E. Freinkman, S. Okuda, N. Ruiz, D. Kahne, Regulated assembly of the transenvelope protein complex required for lipopolysaccharide export. *Biochemistry* **51**, 4800–4806 (2012).
36. M. Zhang *et al*., Rational design of true monomeric and bright photoactivatable fluorescent proteins. *Nat. Methods* **9**, 727–729 (2012).
37. S. A. McKinney, C. S. Murphy, K. L. Hazelwood, M. W. Davidson, L. L. Looger, A bright and photostable photoconvertible fluorescent protein. *Nat. Methods* **6**, 131–133 (2009).
38. J. Elf, G. W. Li, X. S. Xie, Probing transcription factor dynamics at the single-molecule level in a living cell. *Science* **316**, 1191–1194 (2007).
39. B. P. English *et al*., Single-molecule investigations of the stringent response machinery in living bacterial cells. *Proc. Natl. Acad. Sci. U.S.A.* **108**, E365–E373 (2011).
40. P. Mehta *et al*., Dynamics and stoichiometry of a regulated enhancer-binding protein in live Escherichia coli cells. *Nat. Commun.* **4**, 1997 (2013).
41. S. Bakshi, B. P. Bratton, J. C. Weisshaar, Subdiffraction-limit study of Kaede diffusion and spatial distribution in live Escherichia coli. *Biophys. J.* **101**, 2535–2544 (2011).
42. D. Mazza, A. Abernathy, N. Golob, T. Morisaki, J. G. McNally, A benchmark for chromatin binding measurements in live cells. *Nucleic Acids Res.* **40**, e119 (2012).
43. A. Javer *et al*., Short-time movement of E. coli chromosomal loci depends on coordinate and subcellular localization. *Nat. Commun.* **4**, 3003 (2013).
44. A. Gahlmann, W. E. Moerner, Exploring bacterial cell biology with single-molecule tracking and super-resolution imaging. *Nat. Rev. Microbiol.* **12**, 9–22 (2014).
45. T. Y. Chen *et al*., Concentration- and chromosome-organization-dependent regulator unbinding from DNA for transcription regulation in living cells. *Nat. Commun.* **6**, 7445 (2015).